Protein Science

Active site conformational changes upon reaction intermediate biotinyl-5'-AMP binding in biotin protein ligase from Mycobacterium tuberculosis

Journal:	*Protein Science*
Manuscript ID:	PRO-14-0031.R1
Wiley - Manuscript type:	Full-Length Papers
Date Submitted by the Author:	n/a
Complete List of Authors:	Ma, Qingjun; European Molecular Biology Laboratory, Akhter, Yusuf; European Molecular Biology Laboratory, Wilmanns, Matthias; European Molecular Biology Laboratory, Ehebauer, Matthias; European Molecular Biology Laboratory,
Keywords:	BirA, BPL, biotinylation, Mycobacterium tuberculosis, structure

Active site conformational changes upon reaction intermediate biotinyl-5'-AMP binding in biotin protein ligase from *Mycobacterium tuberculosis*

Qingjun Ma[1, 2], Yusuf Akhter[1, 3], Matthias Wilmanns[1], and Matthias T. Ehebauer[1#]

[1] European Molecular Biology Laboratory - Hamburg, c/o DESY, Building 25A, Notkestrasse 85, 22603 Hamburg, Germany.

[2] Present address: Institute for Biochemistry, University of Luebeck, Ratzeburger Allee 160, 23538 Luebeck, Germany.

[3] Present address: School of Life Sciences, Central University of Himachal Pradesh, Dist. Kangra, Himachal Pradesh - 176215, India.

Correspondence: Matthias Ehebauer, European Molecular Biology Laboratory – Hamburg, c/o DESY, Building 25A, Notkestrasse 85, 22603 Hamburg, Germany. Tel: +49-40-89902-126. Fax: +49-40-89902-149. E-mail: ehebauer@embl-hamburg.de

Running title: *M. tuberculosis* BPL

Manuscript pages: 22

Manuscript supplemental material pages: 1

Number of figures: 4

Number of tables: 1

Supplemental material description:

There is one supplemental figure and figure legend showing a multiple sequence

alignment of biotin protein ligase homologs. The figure demonstrates that residues of functional importance identified in the structure are conserved and therefore relevant to the protein family as a whole.

Filename: FigureS1.tiff

Abbreviations: BCCP, biotin carboxyl-carrier protein; BirA, biotin induced repressor A; BME, β-mercaptoethanol; BPL; biotin protein ligase; TEV, tobacco etch virus.

Abstract

Protein biotinylation, a rare form of post-translational modification, is found in enzymes required for lipid biosynthesis. In mycobacteria, this process is essential for the formation of their complex and distinct cell wall and has become a focal point of drug discovery approaches. The enzyme responsible for this process, biotin protein ligase, substantially varies in different species in terms of overall structural organization, regulation of function and substrate specificity. To advance the understanding of the molecular mechanism of biotinylation in *Mycobacterium tuberculosis* we have biochemically and structurally characterized the corresponding enzyme. We report the high-resolution crystal structures of the apo-form and reaction intermediate biotinyl-5'-AMP-bound form of *M. tuberculosis* biotin protein ligase. Binding of the reaction intermediate leads to clear disorder-to-order transitions. We show that a conserved lysine, Lys138, in the active site is essential for biotinylation.

Keywords: *Mycobacterium tuberculosis*, BPL, BirA, biotinylation, crystal structure.

Statement for broader audience:

We have determined the molecular structure of a biotin ligase enzyme from the bacterium that causes tuberculosis. The enzyme is responsible for an essential modification of several other proteins that are important for the proper functioning of the bacterium’s metabolism.

Introduction

Biotin-dependent carboxylases are enzymes that have multiple important metabolic functions (1, 2). These enzymes share a requirement for biotin, which is covalently bound to a biotin carboxyl-carrier protein (BCCP) domain common to all these carboxylases. Biotin protein ligase (BPL, EC 6.3.4.15) catalyses the ATP-dependent ligation of biotin to a BCCP domain, in two reaction steps:

$$(1)\ \text{biotin} + Mg^{2+}\text{-ATP} \rightarrow \text{biotinyl-5′-AMP} + PP_i$$

$$(2)\ \text{biotinyl-5'-AMP} + \text{BCCP} \rightarrow \text{AMP} + \text{biotin-BCCP}$$

In the first reaction biotin and ATP are condensed into the intermediate biotinyl-5'-AMP liberating pyrophosphate. The BPL then recruits BCCP and transfers the biotin from biotinyl-5'-AMP to the BCCP protein substrate. BPL and down-stream enzymes that use biotinylation as covalent modification have recently been investigated as potential drug targets demonstrating the importance of the enzyme for potential medicinal applications and to understand in mechanistic terms the biochemical processes associated with it (3).

Several structures of bacterial and archaeal BPLs have been determined (4-10). The *Escherichia coli* BPL, called the biotin-induced repressor A (BirA), has been extensively studied as a BPL prototype (4-7). *E. coli* BirA is a type II BPL and consists of three domains: an N-terminal DNA-binding domain with a helix-turn-helix motif, a ligase domain with a central β-sheet and a C-terminal SH3-like domain (6). *E. coli* BPL is a bifunctional protein. In addition to its biotin ligase function, it also functions as a biotin synthesis repressor (11). Binding of the BCCP domain and binding of biotin or any analog of the intermediate biotinyl-5'-AMP to *E. coli* BPL are mutually exclusive (12). BPL assembly with BCCP induces BPL dimerization, which in turn leads to binding and subsequent repression of the biotin biosynthesis operon (11,

12).

In contrast, BPLs in thermophilic archaea and mycobacteria are type I BPLs, which lack the N-terminal DNA-binding domain and hence are incapable of regulation at the expression level. The type I BPL catalytic ligase domain and the C-terminal SH3-like domain have a similar structure to those of type II BPLs. Dimerization of some type I BPLs has been reported (8,12), but it is independent of ligand binding and the dimerization interfaces are distinct from those seen in prototypical type II *E. coli* BPL (5, 8, 12). In *M. tuberculosis* BPL (Rv3279c) dimerization under specific crystallization conditions has been observed (13). However, gel filtration and dynamic light scattering data showed that the protein is monomeric in solution (13, 14).

The aim of this study was to add new structural and functional findings on *M. tuberculosis* BPL where data have been missing and to integrate them into a complete and useful picture of this enzyme. We report the first structure of the biotin-5'-AMP-bound form of *M. tuberculosis* BPL at 1.7 Å resolution and compare it to the apo-conformation of the enzyme, which we determined at 1.8 Å resolution. Analysis of these structures revealed substantial conformational changes that took place upon biotin-5'-AMP binding. We validated the active site of *M. tuberculosis* BPL by mutating Lys138 into a serine, which completely abolishes BPL activity.

Results

M. tuberculosis BPL is monomeric irrespective of ligand binding – We used analytical gel filtration to determine the BPL association state in solution (Fig. 1). The molecular weight of the full-length BPL based on its amino acid sequence is approximately 28 kDa. The retention volume of BPL (12.45 ml) from the calibrated gel filtration column gives a molecular weight of 26.7 kDa (Fig. 1A), unambiguously

indicating that the enzyme is monomeric in solution. The elution profile of BPL did not change when the protein is incubated with biotin and ATP implying that it remains monomeric in the presence of these ligands (Fig. 1B). This is in agreement with published data that demonstrate that *M. tuberculosis* BPL is monomeric in solution regardless of which substrate is present (14).

M. tuberculosis BPL structure in the absence and presence of the step 1 reaction product biotinyl-5'-AMP – We have determined the crystal structures of the apo- and biotinyl-5'-AMP-complexed forms of *M. tuberculosis* BPL at 1.8 Å and 1.7 Å resolution, respectively (Fig. 2A, B). The overall structure of the apo- and ligand-bound BPLs is similar with a root mean square deviation in Cα atomic positions of 0.47 Å (Fig. 2C). The overall fold of *M. tuberculosis* BPL is in agreement with a 2.8 Å resolution structure of the apo-form of the enzyme (13). The protein contains two domains in a dumbbell shaped arrangement. At the N-terminal part there is a catalytic domain (residues 1-217), with a BPL-LplA-LipB fold (Pfam family: PF03099). Its central part is a β-sheet consisting of seven strands (β1↑ β2↑ β3↓ β7↑ β6↓ β5↑ β4↓). Five helices flank the β-sheet: α2 is on one side; α1, α3, α4 and α5 are on the other side. The C-terminal SH3-like domain (residues 218-265) is composed of five anti-parallel β-strands (β12↑ β8↓ β9↑ β10↓ β11↑) that form a small β-barrel. In the crystal of the ligand-bound BPL there is well interpretable electron density for biotinyl-5'-AMP, implying that ATP and biotin react to form this product of the first BPL reaction step (Fig. 2D), as previously reported for BPL from *Pyrococcus horikoshii* (9). Three regions that lack electron density in the crystal of apo-BPL, including residues 1-7, 63-77 and 162-171, are evident in biotinyl-5'-AMP-bound BPL (Fig. 2B). The latter two of these segments are near the BPL active site, and their folding is

likely to be induced by biotinyl-5'-AMP binding, as observed in the equivalent enzymes from *E. coli* and *P. horikoshii* (5, 9). This data is also in agreement with the report of an inhibitor-bound *M. tuberculosis* BPL structure in which the same disorder-to-order transition was observed (3). A short helix and loop is formed by residues 162-172, which together with the two additional strands formed by residue segment 63-77, as well as strands β6 and β7 of the central β-sheet, compose the ligand binding pocket. The interactions between biotinyl-5'-AMP and *M. tuberculosis* BPL are similar to those reported for other ligand-bound BPL structures (Fig. 2E, F) (3, 5, 8), demonstrating that biotinyl-5'-AMP binding and hence the overall active site architecture is conserved across type I and type II BPLs. The invariant active site Lys138 tightly interacts with the oxygen atoms of both biotinyl and AMP moieties of biotinyl-5'-AMP (Fig. 2E).

In addition, residues 1-7 form a helix at the N-terminus in the reaction intermediate-bound BPL. As this area is remote from the active site, its folding may be induced by crystal contacts specific to the monoclinic biotinyl-5'-AMP-bound BPL crystal form (*cf*. Table I).

Lys138 is essential for M. tuberculosis BPL activity – We have used a coupled enzyme assay to measure the catalytic activity towards ATP of BPL (Fig. 3A). Wild type BPL is active and its kinetic parameters for ATP consumption are K_M= 0.20 ± 0.04 mM and the k_{cat} = 0.017 s^{-1} (k_{cat}/K_M = 0.085 $s^{-1}mM^{-1}$) (Fig. 3A). The kinetic parameters determined here differ slightly from those reported by Purushothaman *et al*. (14), likely due to the higher concentrations of substrate they assayed in the linear velocity range. A mobility shift assay was employed to measure BCCP biotinylation (Fig. 3C). We subsequently used these assays to test the role of the Lys138 of *M. tuberculosis* BPL. The lysine to serine substitution completely abolishes the ligase

158 activity (Fig. 3B) and renders BPL unable to biotinylate its protein substrate BCCP
159 (Fig. 3C) confirming the essential role of this conserved active site lysine in BPL
160 catalysis.
161

162 **Discussion**

163 In this contribution, we have been able to determine and characterize the BPL
164 structure from *M. tuberculosis* in the presence of the reaction intermediate biotinyl-5'-
165 AMP. This allowed comparison with related structures, in particular with a recent
166 structure of BPL in which the active site is bound by the inhibitor Bio-AMS (3). The
167 structures of both these ligand-bound BPLs are nearly identical, their root mean
168 square deviation of Cα atomic positions being 0.38 Å (Figure 4). The structure of the
169 binding pocket in biotinyl-5'-AMP-bound BPL is also similar to that of *M. tuberculosis*
170 BPL bound by Bio-AMS (compare Fig. 4A and Fig. 4B; 3). Binding of the inhibitor
171 leads to the same type of disorder-to-order transitions that are evident in the
172 structure of BPL bound by the reaction intermediate (3). The two ligands adopt a
173 similar conformation in the active site (Fig. 4D) and the same constellation of
174 hydrogen bonds is formed between their respective ligands and the protein backbone
175 (Fig. 2E; 3). In particular, the active site residue Lys138 is hydrogen bonded to the
176 two ligands in the same manner.
177 Interestingly, the structure of a *M. tuberculosis* apo-BPL from a dehydrated crystal
178 (3L1A) (13) reveals that the residue segments 63-77 and 162-171 are ordered, as
179 observed for *M. tuberculosis* BPL in the presence of the reaction intermediate (Fig.
180 4C). These however adopted a different conformation to both the reaction
181 intermediate and inhibitor-bound forms (Fig. 4D). These differences, although likely
182 biased by enhanced crystal contacts due to crystal dehydration, may indicate that the

biotinyl-5'-AMP disorder-to-order transition is more transient than suggested by a sole binary comparison of the apo- and the biotinyl-5'-AMP-bound forms.

Most residues interacting with the biotinyl moiety have the same conformation in the apo- and the ligand-bound form, whereas the AMP binding residues largely reside in those regions that are disordered in the apo-structure. A reasonable scenario for substrate binding based on our structural data is therefore the following: biotin binds and induces the disorder-to-order transition of residues 63-77, which subsequently supplies important binding sites such as W74, R69 and A75 for binding ATP (Fig. 2E, F); ATP binds and induces the folding of the residues 162-171 (Fig. 2B). Should ATP bind first, its interaction with residues like W74 and R69 may occlude the biotin-binding pocket of the active site. In the ATP-bound structure of *P. horikoshii* BPL (1X01), the ligand pocket is indeed closed by ATP and prevents further binding of biotin (9).

The residue Lys138 has been recognized as a key functional residue in BPLs and other proteins with BPL-LplA-LipB domains (6, 15-17). Lys138 is postulated to orientate the substrates biotin and ATP and stabilize the transition state of the intermediate (8). The *P. horikoshii* BPL mutant $K^{111}A$, analogous to the $K^{138}S$ mutant of *M. tuberculosis* BPL, binds biotin and ATP, but cannot form biotinyl-5'-AMP (9). In that structure the phosphate of ATP is not in the optimal position to react with the biotin carboxyl group. In our ligand-bound BPL structure, Lys138 forms critical hydrogen bonds to the phosphate group of the AMP moiety and the carboxyl group of the biotin moiety (Fig. 2E). The important role of Lys138 in BPL catalysis is strongly supported by all available structural data and is corroborated by our biochemical evidence demonstrating that substitution of this lysine in *M. tuberculosis* BPL abolishes its activity *in vitro*.

Materials and Methods

Cloning, protein expression and purification. The open reading frame of the *M. tuberculosis bpl*/*birA* gene (Rv3279c) was amplified by PCR from genomic DNA using KOD polymerase with the sense primer 5'-AAAACCATGGCCGACCGCGATCGGCTCAG-3' and antisense primer 5'-ATTAGAATTCGCGCGAGTTAACGCAAATGCACCAC-3'. The PCR product was ligated to the *Nco*I and *Eco*RI sites of the expression vector pETM11, which contained an N-terminal poly-histidine tag, which was cleaved from the recombinant fusion protein with tobacco etch virus (TEV) protease. The construct was transformed into *E. coli* Rossetta (DE3)plysS cells for protein expression. Transformed bacteria from a single clone were cultured in Luria-Broth medium containing 50 µg/ml kanamycin at 37°C until the culture reached an optical density of 0.6 at 600 nm. Protein expression was then induced with isopropylthiogalactopyranoside at a final concentration of 0.1 mM and the culture incubated overnight at 20°C. The bacteria were harvested by centrifugation at 3000 x g and 4^{o}C. The culture pellets were resuspended in 20 mM Tris-HCl (pH 8.0), 300 mM NaCl, 10 mM imidazole, 0.02 % (v/v) β-mercaptoethanol (BME), with mini-EDTA-free protease inhibitor (Roche) at concentrations recommended by the manufacturer. Cells were lysed by sonication using a Bandelin Sonoplus HD3200 sonicator set to pulse with an on-off cycle of 0.3 sec - 0.7 sec and an amplitude of 45 % for a total of 3 min. The sample was cooled on ice throughout. The lysate was centrifuged at 38700 x g for 1 hour at 4^{o}C. The supernatant was loaded onto a nickel-nitrilotriacetic acid (Ni-NTA) resin that had a bead volume of 2 ml (Qiagen). The resin was washed with 20 column volumes of 20 mM Tris-HCl (pH 8.0), 300 mM NaCl, 10 mM imidazole, 0.02 % (v/v) BME. Bound

proteins were eluted with 20 mM Tris-HCl (pH 8.0), 200 mM NaCl, 300 mM imidazole, 0.02 % (v/v) BME. The eluted protein was cleaved with 0.5 μM TEV protease overnight at 4°C, while dialyzing against 20 mM Tris-HCl (pH 8.0), 50 mM NaCl, 2 mM dithiothreitol (DTT), 1 mM EDTA. Contaminants in the dialyzed protein solution were removed by reloading the sample onto the Ni-NTA column, which bound the cleaved tag and the protease. The recombinant BPL was collected in the flow-through. The protein was further purified by gel filtration using a Superdex 75 column (GE Healthcare) equilibrated with 10 mM HEPES (pH 7.5), 50 mM NaCl, 1 mM DTT. The column was calibrated using the low molecular weight calibration kit from Amersham. In order to assess if the presence of substrate changed the oligomeric state of BPL we added 40 μM biotin and 3 mM ATP to the purified apo-BPL and incubated these for 30 min before re-loading the sample onto a Superdex 75 column (GE Healthcare). The BPL mutant, $K^{138}S$, was produced in the same manner as apo-BPL. The point mutation was introduced into the BPL coding sequence using the Stratagene site-directed mutagenesis kit using standard protocols recommended by the manufacturer.

***X-ray structure determination*.** All crystals used in this study were grown by the hanging drop vapor diffusion method at 20°C. Apo-BPL crystals grew in drops composed of 0.1 M Tris-HCl (pH 8.5), 0.2 mM trimethylamine N-oxide, 20 % (w/v) PEG-2000 monomethyl ether. The crystallization drop was prepared by mixing 1 μl of this solution with 1 μl of 15 mg/ml apo-BPL in 10 mM HEPES (pH 7.5), 50 mM NaCl, 1 mM DTT. Crystals of the biotinyl-5'-AMP-BPL complex were grown from equal volumes of 10 mM biotin, 10 mM ATP and 21 mg/ml BPL incubated at 37°C for 30 min prior to setting up the crystallization drop. The drop was prepared by mixing 6 μl

of this sample with 1 µl well solution composed of 0.1 M Tris-HCl (pH 7.8), 0.2 M Li_2SO_4, 25 % (w/v) PEG-4000. The crystals were mounted in loops directly from the drop, without cryo-protectant, and flash frozen in liquid nitrogen. X-ray diffraction datasets were collected at 100K, using the synchrotron radiation beam line BW7A of the DORIS storage ring at EMBL/DESY, Hamburg, Germany. The data were processed with Denzo & Scalepack (18).

The apo-BPL structure was solved by molecular replacement using CaspR (19) and the *E. coli* BirA structure 1HXD as the search model. Atomic positions and individual isotropic B-factors were refined using the default geometric restraints of the program Refmac5 (20). TLS tensors were used to model the anisotropic effect. Five percent of the unique reflections were excluded form refinement and served as data for cross-validation to monitor model fitting. Model building between refinement cycles was performed with XtalView (21). The diffraction and refinement statistics are summarized in Table I. Residues 8-64, 77-162, 171-265 of chain A, and residues 8-65, 77-163, 169-265 of chain B could be modeled on electron density.

The structure of the biotinyl-5'-AMP-BPL complex was solved by molecular replacement using the refined apo-structure as search model, using the same refinement and modeling procedure as for the apo-structure. Geometric restraints of biotinyl-5'-AMP used during refinement and model building were generated using PRODRG (22). All graphic representations of models were created using PyMol (23).

Electrophoretic mobility shift assay. After the first affinity chromatography step BPL was further purified by gel filtration using as buffer 10 mM Tris-HCl (pH 7.5), 0.1 mM DTT, 5 % (v/v) glycerol, 200 mM KCl. A transformed *E. coli* strain containing a BCCP domain expression plasmid was grown in Luria-Broth media and purified as described (24). The recombinant BCCP domain contains the 87 C-terminal residues

of *E. coli* BCCP (26) and has a molecular weight of 9.3 kDa. The recombinant BCCP domain was concentrated by vacuum drying to 60 μM. The biotinylation reaction was performed as described in (24). The biotinylation reaction mixture contained 40 mM Tris-HCl (pH 8.0), 3 mM ATP, 5.5 mM $MgCl_2$, 1 mM DTT, 100 mM KCl, 60 μM BCCP, 40 μM biotin and 2 μM or 8 μM of wild type BPL or $K^{138}S$. The proteins were pre-incubated for 20 min at 20°C and their mobility was analyzed in an 8% Tris-borate-EDTA native polyacrylamide gel.

Enzyme activity assay. We used a coupled enzyme assay that measured the quantity of AMP released during the second step of BPL's reaction (25). Spectrophotometric data were recorded using a PowerWaveX Select spectrophotometer (Bio-Tek Instruments) and Greiner Bio-one UV-transparent, flat-bottom 96-well plates. Data was recorded using KC4 Kineticalc version 3.01 (Bio-Tek Instruments) and analyzed using GraphPad Prism 5 version 5.03 (Graphpad Software Inc.). The final concentration of reagents in one 300 μl reaction volume was 2.5 mM phosphoenolpyruvate, 0.2 mM NADH, 11.5 U myokinase, 9.9 U pyruvate kinase, 12.3 U lactate dehydrogenase, 100 μM biotin, 100 μM BCCP, 80 mM Tris-HCl (pH 8.0), 400 mM KCl, 11 mM $MgCl_2$, 0.2 mM DTT, and 0.2 mg/ml bovine serum albumin. The concentration of ATP was varied between 0.1-4 mM. The concentration of protein used in each reaction was 10 nM BPL or $K^{138}S$. The reaction was initiated upon addition of biotin and the consumption of NADH monitored at 340 nm at 30°C for 1 hour.

Electronic supplementary material

Figure S1. Structure-annotated multiple sequence alignment of BPLs form different

species. The secondary structure elements are labeled according to the apo-structure of *M. tuberculosis* BPL (2CGH). Additional secondary structures that are the result of disorder-to-order transitions upon biotinyl-5′-AMP binding in *M. tuberculosis* BPL are framed by red boxes. Residues involved in ligand binding are labeled with a dot. Residues that form hydrogen bonds between the ligand and their side chains are indicated with a green dot, those that form hydrogen bonds between the ligand and their backbone atoms are in orange and W74 that forms stacking interactions with the adenylate-moiety of the ligand is in blue.

Acknowledgments

We thank the lab of Stefan H.R. Kaufmann of the Max-Planck Institute of Infection Biology, Berlin, Germany, for the gift of *M. tuberculosis* genomic DNA and John E. Cronan of the University of Illinois, Urbana, USA, for the *E. coli* strain expressing the BCCP domain. We thank EMBL staff for support at beam line BW7A at EMBL/DESY, Hamburg, Germany. We also thank Arie Geerlof for his assistance with the enzymatic assay. YA and MTE were supported by EMBO long-term fellowships (ALTF 768-2010 and ALTF 727-2008). This work was supported by the European Commission grant FP7-HEALTH_2009-241587, awarded to MW.

Accession code:

The coordinates of these structures have been deposited into the Protein Data Bank with the accession number 2CGH for apo-BPL and 4OP0 for biotinyl-5’-AMP-BPL.

References

1. Cronan JE Jr, Waldrop GL (2002) Multi-subunit acetyl-CoA carboxylases. Prog Lipid Res 41:407-435.

2. Tong L (2013) Structure and function of biotin-dependent carboxylases. Cell Mol Life Sci 70:863-891.

3. Duckworth BP, Geders TW, Tiwari D, Boshoff HI, Sibbald PA, Barry 3rd CE, Schnappinger D, Finzel BC, Aldrich CC (2011) Bisubstrate adenylation inhibitor of biotin protein ligase from Mycobacterium tuberculosis. Chem Biol 18:1432-1441.

4. Barker DF, Campbell AM (1981a) The *birA* gene of *Escherichia coli* encodes a biotin holoenzyme synthase. J Mol Biol 146:451-467.

5. Wood ZA, Weaver LH, Brown PH, Beckett D, Matthews BW (2006) Co-repressor induced order and biotin repressor dimerization: a case for divergent followed by convergent evolution. J Mol Biol 357:509-523.

6. Wilson KP, Shewchuk LM, Brennan RG, Otsuka AJ, Matthews BW (1992) *Escherichia coli* biotin holoenzyme synthetase/bio repressor crystal structure delineates the biotin- and DNA-binding domains. Proc Natl Acad Sci USA 89:9257-9261.

7. Weaver LH, Kwon K, Beckett D, Matthews BW (2001) Corepressor-induced

organization and assembly of the biotin repressor: a model for allosteric activation of a transcriptional regulator. Proc Natl Acad Sci USA 98:6045-6050.

8. Bagautdinov B, Kuroishi C, Sugahara M, Kunishima N (2005) Crystal structure of biotin protein ligase from *Pyrococcus horikoshii* OT3 and its complexes: structural basis of biotin activation. J Mol Biol 353:322-333.

9. Bagautdinov B, Matsuura Y, Bagautdinova S, Kunishima N (2008) Protein biotinylation visualized by a complex structure of biotin protein ligase with a substrate. J Biol Chem 283:14739-14750.

10. Tron CM, McNae IW, Nutley M, Clarke DJ, Cooper A, Walkinshaw MD, Baxter RL, Campopiano DJ (2009) Structural and functional studies of the biotin protein ligase from *Aquifex aeolicus* reveal a critical role for a conserved residue in target specificity. J Mol Biol 387:129-146.

11. Barker DF, Campbell AM (1981b) Genetic and biochemical characterization of the *birA* gene and its product: Evidence for a direct role of biotin holoenzyme synthase in repression of the biotin operon in *Escherichia coli.* J Mol Biol 146:469-492.

12. Daniels KG, Beckett D (2010) Biochemical properties and biological function of monofunctional microbial biotin protein ligase. Biochemistry 49:5358-5365.

13. Gupta V, Gupta RK, Khare G, Salunke DM, Surolia A, Tyagi AK (2010) Structural ordering of disordered ligand-binding loops of biotin protein ligase into active

conformations as a consequence of dehydration. PLoS ONE, 5:e9222.

14. Purushothaman S, Gupta G, Srivastava R, Ganga Ramu V, Surolia A (2008) Ligand specificity of group I biotin protein ligase of *Mycobacterium tuberculosis*. PLoS ONE 3:e2320.

15. Reche PA (2000) Lipoylating and biotinylating enzymes contain a homologous catalytic module. Protein Sci 9:1922-1929.

16. Ma Q, Zhao X, Nasser Eddine A, Geerlof A, Li X, Cronan JE, Kaufmann SH, Wilmanns M (2006) The *Mycobacterium tuberculosis* LipB enzyme functions as a cysteine/lysine dyad acyltransferase. Proc Natl Acad Sci USA 103:8662-8667.

17. Chapman-Smith A, Cronan JE Jr (1999) The enzymatic biotinylation of proteins: a post-translational modification of exceptional specificity. Trends Biochem Sci 24:360-363.

18. Otwinowski Z, Minor W (1997) Processing of X-ray diffraction data collected in oscillation mode. Methods Enzymol 276:307-326.

19. Claude JB, Suhre K, Notredame C, Claverie JM, Abergel C (2004) CaspR: a web server for automated molecular replacement using homology modelling. Nucleic Acids Res 32:W606-609.

20. Murshudova GN, Vagin AA, Dodson EJ (1997) Refinement of macromolecular

406 structures by the maximum-likelihood method. Acta Cryst D53:240-255.
407
408 21. McRee DE (1999) XtalView/Xfit-A versatile program for manipulating atomic
409 coordinates and electron density. J Struct Biol 125:156-165.
410
411 22. Schuttelkopf AW, van Aalten DMF (2004) PRODRG - a tool for high-throughput
412 crystallography of protein-ligand complexes. Acta Cryst D60:1355-1363.
413
414 23. DeLano WL (2002) The PyMOL Molecular Graphics System, DeLano Scientific,
415 San Carlos, CA, USA. http://www.pymol.org.
416
417 24. Chapman-Smith A, Morris TW, Wallace JC, Cronan JE Jr (1999) Molecular
418 recognition in a post-translational modification of exceptional specificity. Mutants of
419 the biotinylated domain of acetyl-CoA carboxylase defective in recognition by biotin
420 protein ligase. J Biol Chem 274:1449-1457.
421
422 25. Guchhait R, Polakis SE, Dimroth P, Stoll E, Moss J, Lane MD (1974) Acetyl
423 coenzyme A carboxylase system of *Escherichia coli*. J Biol Chem 249:6633-6645.
424
425 26. Chapman-Smith A, Turner DL, Cronan JE Jr, Morris TW, Wallace JC (1994)
426 Expression, biotinylation and purification of a biotin-domain peptide from the biotin
427 carboxy carrier protein of *Escherichia coli* acetyl-CoA carboxylase. Biochem J
428 302:881-887.

Table I: X-ray structure determination and refinement statistics.

Crystals	apo-BPL	biotinyl-5'-AMP-BPL
Wavelength (Å)	0.9364	0.9762
Space group	$P2_12_12_1$	$P2_1$
Cell dimensions (Å) and angles (°)	a = 62.1, b = 81.0, c = 101.9	a = 41.7, b = 75.4, c = 77.6, β = 97.9
Resolution range [a]	39.4-1.80 (1.90-1.80)	31.4-1.70 (1.80-1.70)
Total unique reflections	48344	51119
Completeness (%) [a]	99.8 (99.9)	97.4 (95.9)
Mean I/σ(I) [a]	36.3 (3.9)	15.6 (3.2)
Multiplicity [a]	16.0 (8.5)	12.0 (7.1)
R_{int} (%) [a]	4.4 (55.9)	9.8 (52.6)
R_{sigma} [b] (%) [a]	1.7 (26.2)	4.1 (31.1)
Refinement statistics		
Reflections	45951	48546
R_{work}/R_{free} (%) [a]	18.5 (22.4)	19.5 (24.4)
Number of atoms		
protein	3868	4197
ligand	-	76
solvent	342	340
Relative mean square deviation from standard values		
Bond length (Å)	0.018	0.016
Bond angle (°)	1.78	1.82
Ramachandran plot		
most favored regions	92.2	91.2

additional allowed regions 7.8	8.4
generously allowed regions	0.5

a, Values in parenthesis are for the highest resolution shell.

b, R_{sigma} = Σ[sigma ($|Fo|^2$)]/Σ[$|Fo|^2$]. $|Fo|^2$ are intensities of the merged reflections, referred to in the SHELX-97 manual.

Figure Legends

Figure 1. BPL is a monomer in solution. A, Elution profile of BPL from an analytical gel filtration column calibrated with mass standards (inset). BPL elutes in a volume of 12.45 ml with an apparent molecular weight of a monomer. B, Elution profile of BPL in the presence of 40μM biotin and 3mM ATP. BPL elutes in a volume of 12.04 ml. There is only a minor change in the peak position implying that BPL remains monomeric in the presence of ligand.

Figure 2. Structures of apo- and biotinyl-5'-AMP-bound BPL. A, Apo-BPL (2CGH). The catalytic domain is colored green and the C-terminal SH3-like domain is colored blue. Secondary structure elements are labeled. B, The structure of biotinyl-5'-AMP-bound BPL (4OP0). The domains are colored as in A. Sequence segments undergoing disorder-to-order transitions, when comparing the apo and biotinyl-5'-AMP-bound structures of *M. tuberculosis* BPL, are colored red and their residue range is given. Biotinyl-5'-AMP is shown as a stick model. C, The apo- and biotinyl-5'-AMP-bound BPL structures superposed. D, The electron density map of biotinyl-5'-AMP is shown in black ($2mF_o$-DF_c map contoured at the 1σ level). E, Schematic representation of the BPL active site generated by LIGPLOT (www.ebi.ac.uk/thornton-srv/software/LIGPLOT). Residues are labeled according to the sequence of 4OP0. Carbon atoms are colored black, oxygen atoms red, nitrogen atoms blue, sulfur is yellow and the phosphorus atom is colored orange. F, BPL active site with the side chains of key residues shown by stick presentation.

Figure 3. BPL $K^{138}S$ is inactive. A, Steady state kinetics of BPL for its substrate ATP.

485 BPL reaction velocities are plotted against the increasing concentration of ATP. B,
486 Measurement of BPL activity. The decrease in OD_{340} is a reflection of BPL activity,
487 measured by the consumption of NADH. No decrease is evident in the mutant $K^{138}S$.
488 C, Electrophoretic mobility shift in a non-denaturing polyacrylamide gel assessing the
489 ability of BPL to biotinylate BCCP. All reactions contained BCCP, ATP and biotin as
490 substrates. Biotinylation of BCCP results in increased mobility toward the anode (26).
491 Lane 1, in the absence of BPL there is no biotinylation of BCCP. Lane 2 and 3 show a
492 shift due to biotinylation of BCCP catalyzed by wild type BPL at two concentrations, 2
493 μM and 8 μM BPL, respectively. Lanes 4 and 5 contained samples of the same
494 reactions as in lane 2 and 3, however, the wild type BPL was substituted with the
495 mutant $K^{138}S$ at the two concentrations, 2 μM and 8 μM.
496
497 **Figure 4.** Comparison of *M. tuberculosis* BPL structures. A, Structure of the biotinyl-
498 5'AMP-bound BPL (4OP0) shown as a reference structure for those depicted in B
499 and C. These are shown separately for clarity. Colors and labels are those used in
500 Figure 2. B, Structure of BPL bound by the inhibitor Bio-AMS (3RUX; 3). C, Structure
501 of dehydrated BPL (3L1A; 13). Regions that undergo disorder-to-order transitions in
502 ligand-bound BPL are colored red. D, All three BPL structures superposed. Only
503 those regions adopting structure in the presence of ligand are depicted, as are the
504 superposed biotinyl-5'-AMP and Bio-AMS. The root mean square deviation of Cα
505 atomic positions between 4OP0 and 3RUX is 0.38 Å and that between 4OP0 and
506 3L1A is 0.64 Å.
507

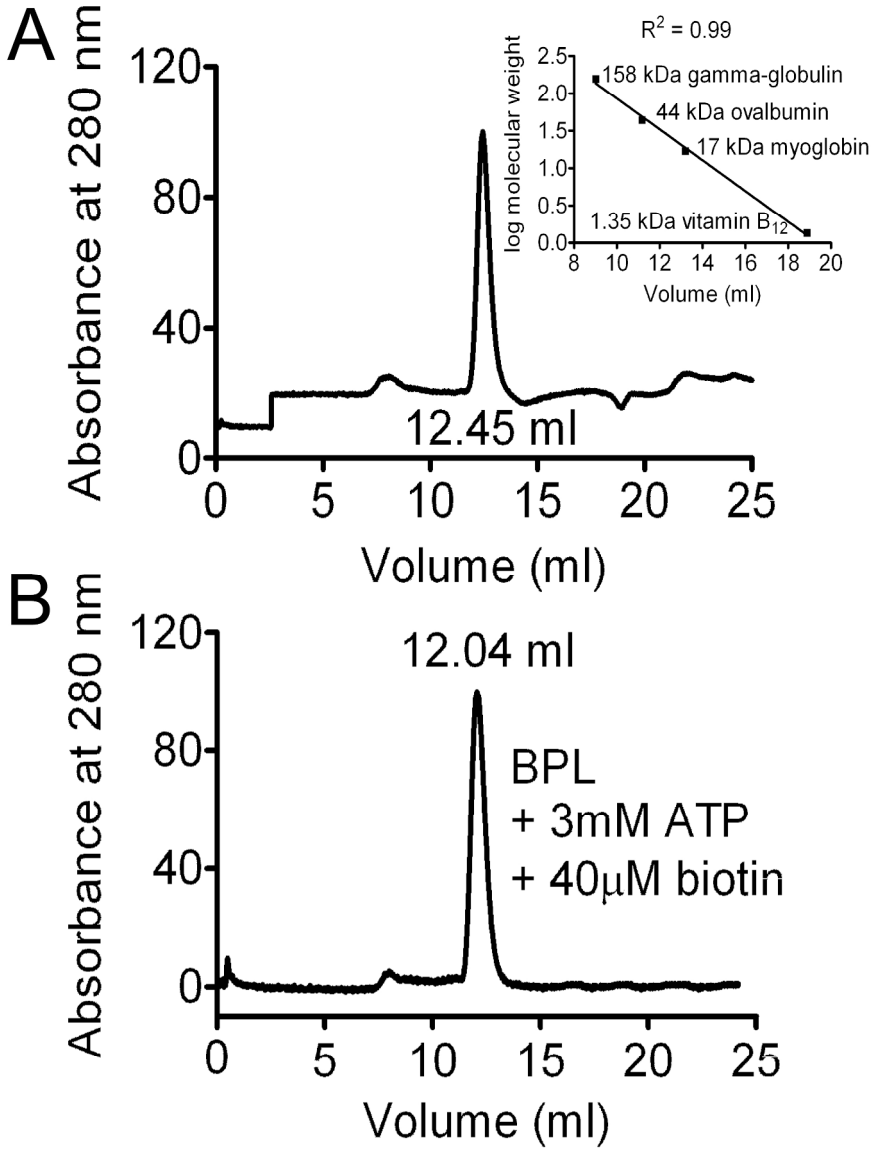

209x283mm (300 x 300 DPI)

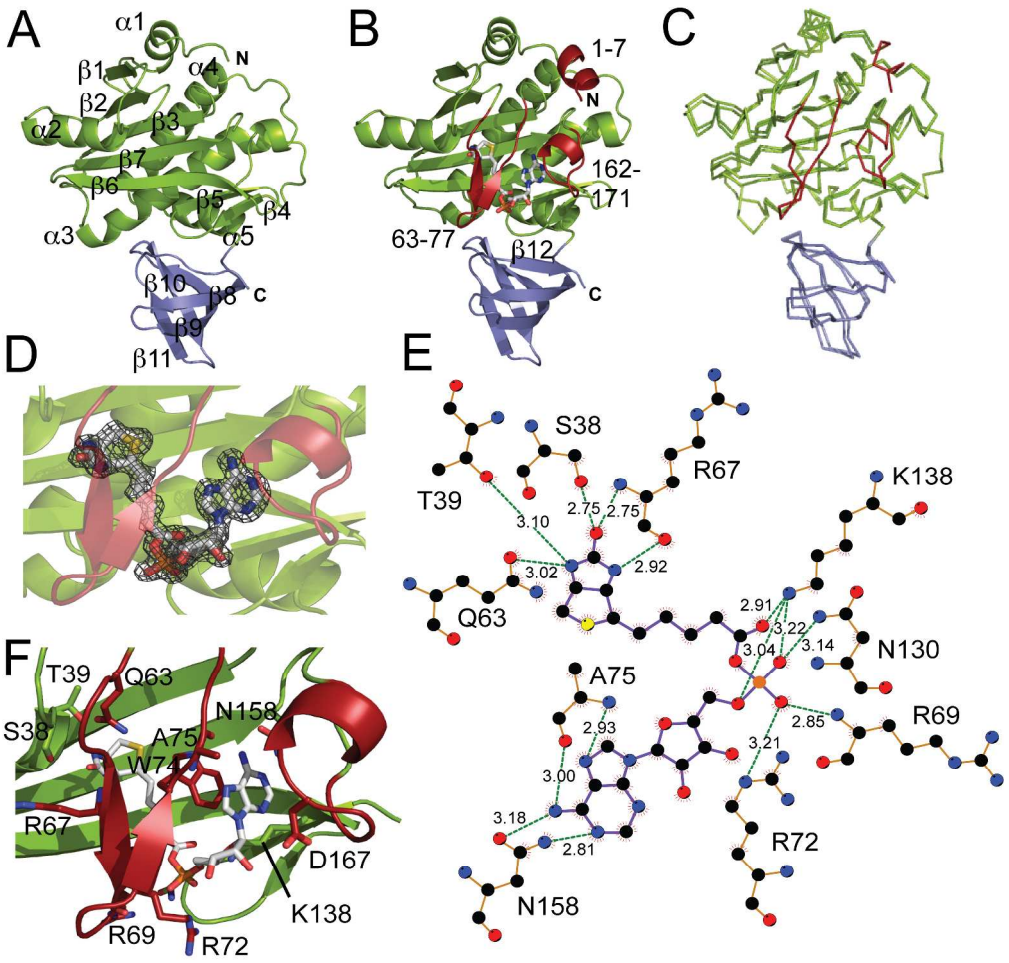

335x324mm (300 x 300 DPI)

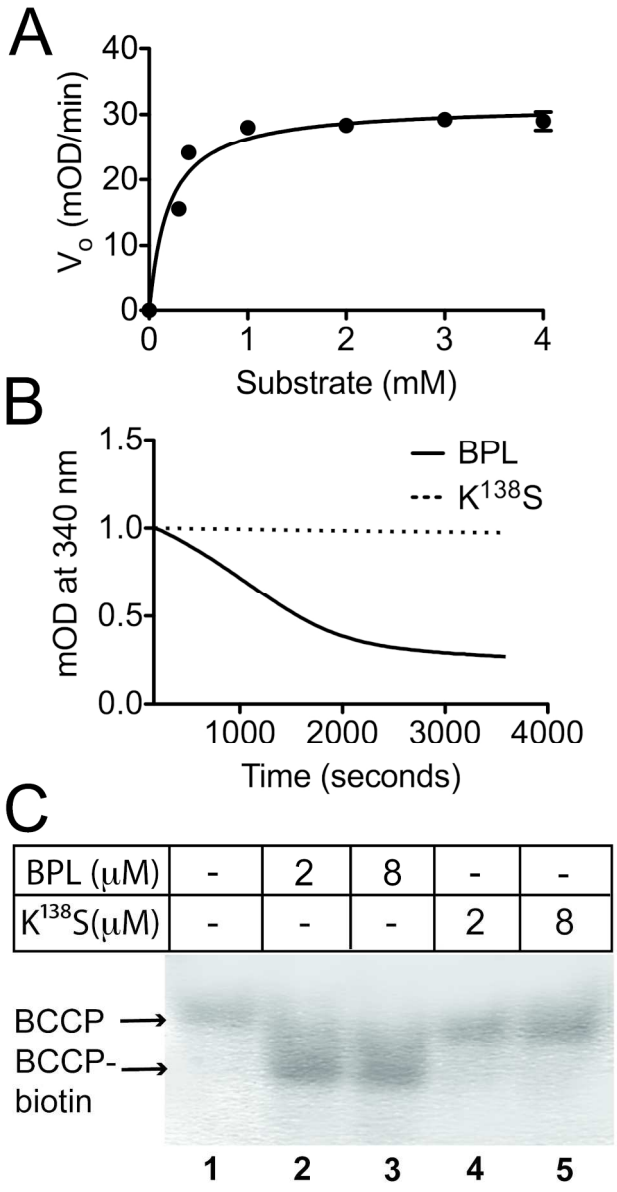

125x232mm (300 x 300 DPI)

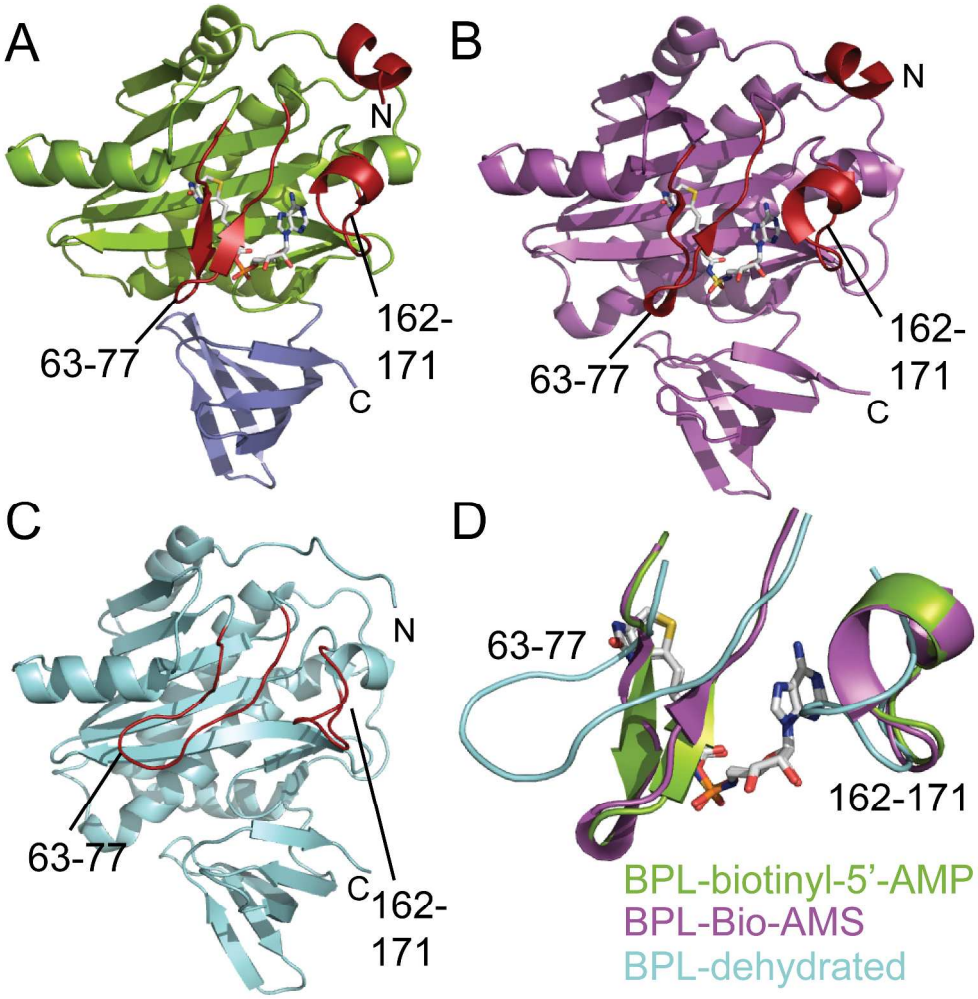

323x323mm (300 x 300 DPI)

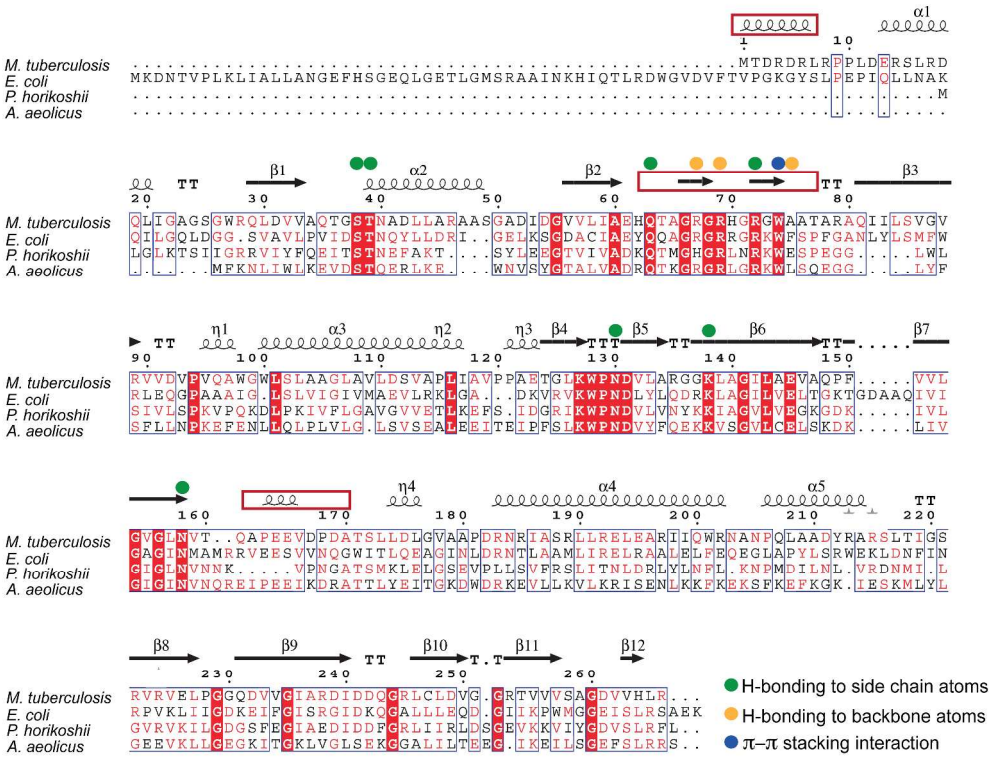

405x323mm (300 x 300 DPI)